Article:
Ghaemi, B, Shaabani, E, Najafi-Taher, R et al. (4 more authors) (2018) Intracellular ROS Induction by Ag@ZnO Core–Shell Nanoparticles: Frontiers of Permanent Optically Active Holes in Breast Cancer Theranostic. ACS Applied Materials and Interfaces, 10 (29). pp. 24370-24381. ISSN 1944-8244

https://doi.org/10.1021/acsami.8b03822

Intracellular ROS Induction by Ag@ZnO Core-Shell Nanoparticles: Frontiers of Permanent Optically Active Holes in Breast Cancer Theranostic

Behnaz Ghaemi [a], Elnaz Shaabani [a#], Roqya Najafi-Taher [a#], Saeedeh Jafari Nodooshan [b], Amin Sadeghpour [c], Sharmin Kharrazi [a*], Amir Amani [a, d*]

[a] *Department of Medical Nanotechnology, School of Advanced Technologies in Medicine (SATiM), Tehran University of Medical Sciences,1417755469 Tehran, Iran*

[b] *Department of Medical Biotechnology, School of Advanced Technologies in Medicine (SATiM), Tehran University of Medical Sciences, 1417755469 Tehran, Iran*

[c] *Centre for X-Ray analytics, department of Material Meet Life, Swiss Federal Laboratories for Material Science and Technology (Empa), 9014 St. Gallen, Switzerland*

[d] *Medical Biomaterials Research Center (MBRC), Tehran University of Medical Sciences, 1417755469 Tehran, Iran*

 # Authors contributed equally in this work

*****Corresponding authors: *sh-kharrazi@tums.ac.ir (S.K.)* and aamani@tums.ac.ir (A.A.)

Keyword. ROS Generation, Ag@ZnO Nanoparticle, Metal-Semiconductor Interfaces, Optically active hole, Apoptosis cascade

Abstract

In this study, we investigated whether ZnO coating on Ag nanoparticles tunes electron flux and hole figuration at Metal-semiconductor interface under UV radiation. This effect triggers photo activity and generation of reactive oxygen species (ROS) from Ag@ZnO nanoparticles which results in enhanced cytotoxic effects and apoptotic cell death in human breast cancer cells (MDA-MB231). In this context, up-regulation of apoptotic cascade proteins (*i.e.* Bax/Bcl2 association, p53, Cytochrome C and caspase-3) along with activation of oxidative stress proteins suggested occurrence of apoptosis by Ag@ZnO NPs in cancer cells through mitochondrial pathway. Also, pre-incubation of breast cancer cells with Ag@ZnO NPs in dark conditions muted NPs-related toxic effects and consequent apoptotic fate, highlighting biocompatible properties of un-excited Ag@ZnO NPs. Furthermore, diagnostic efficacy of Ag@ZnO NPs as CT/optical nano-probes was investigated. Results confirmed the efficacy of the photo-activated system in obtaining desirable outcomes from CT/optical imaging which, represents novel theranostic NPs for simultaneous cancer imaging and therapy.

Introduction

Application of nanotechnology in biomedical sciences is widely expected to change the landscape of treatment and diagnosis . While researchers are faced with tremendous challenges in controlling cell-nanoparticles interactions, novel metallic nanoparticles have attracted important attention because of their unique interactions with biological entities [1]. Advances in development of metallic nanoparticles are being translated into more selective and effective treatment of cancer as well as antibacterial threats [2]. Among metallic nanostructures, silver NPs are the most frequently used ones because of their potent properties in inducing cell death mechanisms [3-4]. These mechanisms help nanoparticles to overcome multi drug resistance (MDR), resulting in improvement of treatment efficiency[5]. However, such nanoparticles address promising therapeutic candidates, whose toxic effects are not limited to the target cells. Over the past few years, energy transfer between quantum dots and their neighbor conjugations has proven to be a very useful tool in many photochemical investigations. Recent studies have revealed that optical properties of ZnO and silver NPs, as isolated systems, are determined by excitons and plasmons, respectively[6]. In core/shell structures, a very thin shell layer of a semiconductor can enhance plasmonic features of the core via plasmon-excitons coupling[7]. A direct contact between ZnO and Ag can result in interfacial processes of charge transfer which are the most important aspects for photocatalytic reactions. Furthermore, when an external ultra violet radiation interacts with these nanoparticles, they can generate radicals in the environment[8]. ROS induction in cancer cells trigger the activation of pro-apoptotic enzymes for development of apoptosis and cell death which is more effective in photodynamic therapy with localized radiation exposure[9]. A composite structure of silver NPs, covered by ZnO as a semiconductor shell, is proposed to achieve a core/shell nanoparticle with novel and special optical/electronic and biomedical properties. A preliminary study has demonstrated special properties of the $Ag@TiO_2$ clusters to store electrons under UV-irradiation and discharge them

in the dark [10]. Another research has shown that interfacial charge exchange between the metal and the semiconductor has a substantial role in defining the photoactivity of the composite[11]. Furthermore, these metal@semiconductor core-shell clusters have photocatalytic activities and are appropriate to promote light-triggered electron-transfer reactions[10]. Au@ZnO core-shell nanoparticles have great potentials for optical-based molecular reactions which could pave the way for planning new optical based nanocomposites for application in chemical sensing[12]. Additionally, nano-based platforms could provide a valuable opportunity to improve dynamic contrast-enhanced imaging techniques for diagnosis of cancers or tracing the target cells by multimodal theranostic agents[13]. Therefore, Ag@ZnO NPs could be introduced as multifunctional nanoparticles for treatment of cancer (via ROS generation) while at the same time can be useful contrast agents for optical and computed tomography (CT-Scan) dual-mode imaging[14].

In this project Ag@ZnO NPs were synthesized and well characterized with transmission electron microscopy (TEM), UV-visible spectroscopy, X-ray diffraction (XRD) and small angle X-ray spectroscopy (SAXS). Also, release of Ag^+ ions from Ag@ZnO NPs and bare Ag NPs was studied over 75 days. Breast cancer (MDA-MB231) and healthy lung fibroblast (MRC5) cells were treated with different concentrations of ZnO, Ag and Ag@ZnO nanoparticles under UV radiation to determine cytotoxic effects and apoptosis pathways. Furthermore, intracellular ROS generation of Ag@ZnO NPs in dark condition and under UV radiation was assessed, followed by evaluation of superoxide dismutase (SOD) and glutathione reductase (GR) enzymes as a measure of cell response to oxidative stress. Moreover, mechanisms of damaged caused by ROS and apoptosis pathways were assessed by measurement of P53, Bax/bcl2 Ratio, caspase 3 and cytochrome C. Additionally, the efficiency of Ag@ZnO NPs as simple and versatile contrast agent for optical/CT imaging was evaluated.

Results & Discussion

Size, Composition, Structure and Analytical Characterization of Ag@ZnO NPs

In order to obtain an effective multifunctional nanoparticle as a novel platform with anticancer and imaging contrast enhancement properties, spherical Ag@ZnO NPs were synthesized. Figure 1 schematically illustrates the ability of the Ag@ZnO NPs to store electrons under UV-radiation and discharge them on demand in dark. ZnO shell coated on Ag NPs, undergoes Fermi level equilibration and following the UV-excitation the efficiency of charge-transfer process is enhanced[15]. The photo-induced charge separation in the semiconductor shell is followed by electron injection into the metal core (Figure 1B). The stored electrons and more likely holes are transferred to an environmental electron/hole acceptor and produce radicals [16]. Moreover, As the electrons from the metal core are discharged, the original surface plasmon absorption of the metal core is restored [17].

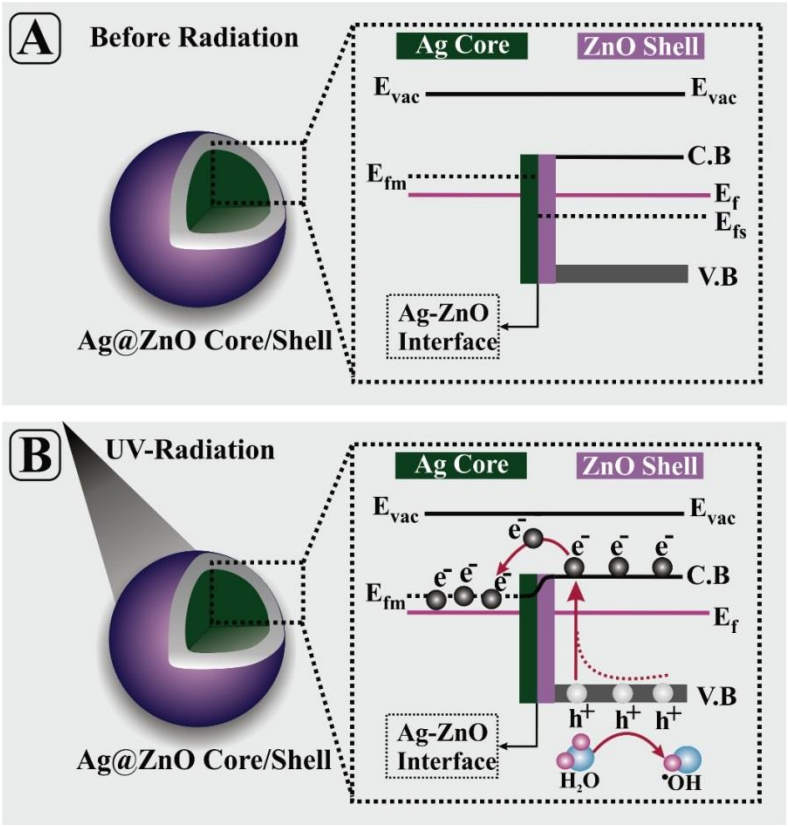

Figure 1. Schematic representation of band structure of Ag/ZnO junction and Fermi energy level equilibrium. As fermi energy level of ZnO (E_{fs}) is lower than that of Ag (E_{fm}), electrons from Ag are transferred to ZnO until the two systems achieve equilibrium with forming a new

Fermi energy level (E_f) (A). Schematic of proposed charge separation process and photocatalytic mechanism of Ag@ZnO NPs after excitation with UV radiation. Due to the higher energy level of ZnO conduction band than the newly formed Fermi energy level of E_f, the photo activated electrons are transferred to the metallic Ag at the interface. Then, the holes are transferred to the surface of semiconductor to catch the electron from environmental molecules (specifically, H_2O and O_2) and Produce ROS (B).

Figure 2A schematically represents the main steps of producing Ag@ZnO NPs. Zn^+ ions are adsorbed onto the surface of negatively charged citrate coated Ag NPs through electrostatic interactions and reacted with NaOH to allow direct formation of ZnO shell on the surface of Ag NP core. The synthesized NPs are calcined at 550℃ in order to obtain a better crystallization and a gradual formation of continuous ZnO shell during the annealing process [18]. TEM (transmission electron microscopy) micrograph and corresponding size distribution analysis of Ag@ZnO NPs after heat treatment show spherical morphologies with an average size of 16 nm along with mean thickness of 3 nm for ZnO shell (Figure 2 B, C and S1). Moreover, dynamic light scattering (DLS) studies of the dispersed NPs showed a mean size of 30 nm and 70 nm in water and DMEM cell culture media, respectively (Figure S2 A and B). UV-Vis absorption spectra of Ag NPs (~ 15nm), ZnO NPs (~ 3nm) and Ag@ZnO (~ 18nm) NPs in the region of 200-800 nm exhibit an absorption peak at ~ 420, 320 and 360 nm, respectively (Figure 2 D). absorption at 320 nm can be assigned to absorption edge of ZnO NPs, while the 420 nm can be attributed to the characteristic surface plasmon resonance of metallic silver [19]. By means of electrodynamic calculations based on Mie theory for coated spheres, and applying the Maxwell–Garnett effective medium theory to calculate the average dielectric constant of the shell, it was possible to both qualitatively and quantitatively, describe the changes in the UV-vis spectra as a consequence of the ZnO shell formation over the Ag NP [20]. The powder XRD patterns of ZnO NPs and calcined Ag@ZnO NPs are shown in Figure 2E from which Ag@ZnO NPs can be identified. The diffraction peaks can be indexed to hexagonal wurtzite ZnO, whereby no diffraction peak from any other impurity is detected. It indicates that Ag@ZnO

NPs have good crystal quality, with some typical and sharp peaks of ZnO at 2-theta values. The peaks of Ag indicate strong interfacial interactions between ZnO and Ag, which is in accordance with the results of TEM [21]. In addition, study of the XRD pattern of Ag@$Zn(OH)_2$ has shown peaks corresponding to orthogonal $Zn(OH)_2$ (Figure S3).

The small angle X-ray scattering (SAXS) has been performed to structurally characterize the nanoparticles in nanometer range. The experimental scattering patterns and the corresponding simulated curves from Ag core and the Ag@ZnO NPs are shown in Figure 2F. We have applied a polydisperse hard sphere and the polydisperse core-shell model for the simulation of scattering curves from Ag core and the Ag@ZnO core-shell NPs, respectively. Therefore, we obtained a core size of 15.6 nm and the shell thickness of 3.0 nm. It is worth to mention that, in order to simulate the scattering curves, we had to consider an asymmetric size distribution function (Schultz distribution) with quite high polydispersity, i.e. 0.6 and 1.0 for the core and the core-shell particles respectively). These finding are in a good agreement with our observations from TEM images.

Although there are many contradictory findings reporting toxicity of silver NPs, literature reveal that its cytotoxicity mainly depends on the release of Ag^+ ions and ROS generation[22]. Since it has been shown that release of Ag^+ ions is the main toxicity mechanism on human cells [23], it was tried to synthesize a tight shell of ZnO to minimize or eliminate release of Ag^+ ions , in addition to enhancing the photocatalytic properties of Ag@ZnO NPs [24]. So, characterization of Ag^+ release is critical for understanding the environmental fate, toxicity, and biomedical impacts of Ag NPs. In these regards, release of silver ion from Ag@ZnO NPs was evaluated every 5 days for a total of 75 days and the results were compared with that of Ag NPs. Obtained results did not show any significant release of Ag^+ ions form Ag@ZnO NPs, while 70% of silver was released from Ag NPs, as illustrated in Figure 2G. Reports indicate that surface coating significantly determines Ag^+ ions related-process kinetics in Ag NPs [25]. A previous

report demonstrated that 16%-20% Ag^+ ions was released from PVP/ PEG-coated Ag NPs after 2 h, while the release of Ag^+ ions for gelatin, citrate and chitosan coated Ag NPs was about 1-3% for 2 h. Thus, the role of polymer coating in controlling the release appears to be minor, acting as a reservoir of Ag^+ which may subsequently be released [26]. Furthermore, polymers may quench generation of ROS from silver NPs and decrease the anticancer efficiency of Ag NPs [27]. Results of our research indicate that Ag@ZnO NPs remained stable for 75 days without any significant Ag^+ release. It seems that the tight-crystal structure of ZnO shell could completely prevent release of Ag^+ ions from Ag@ZnO NPs.

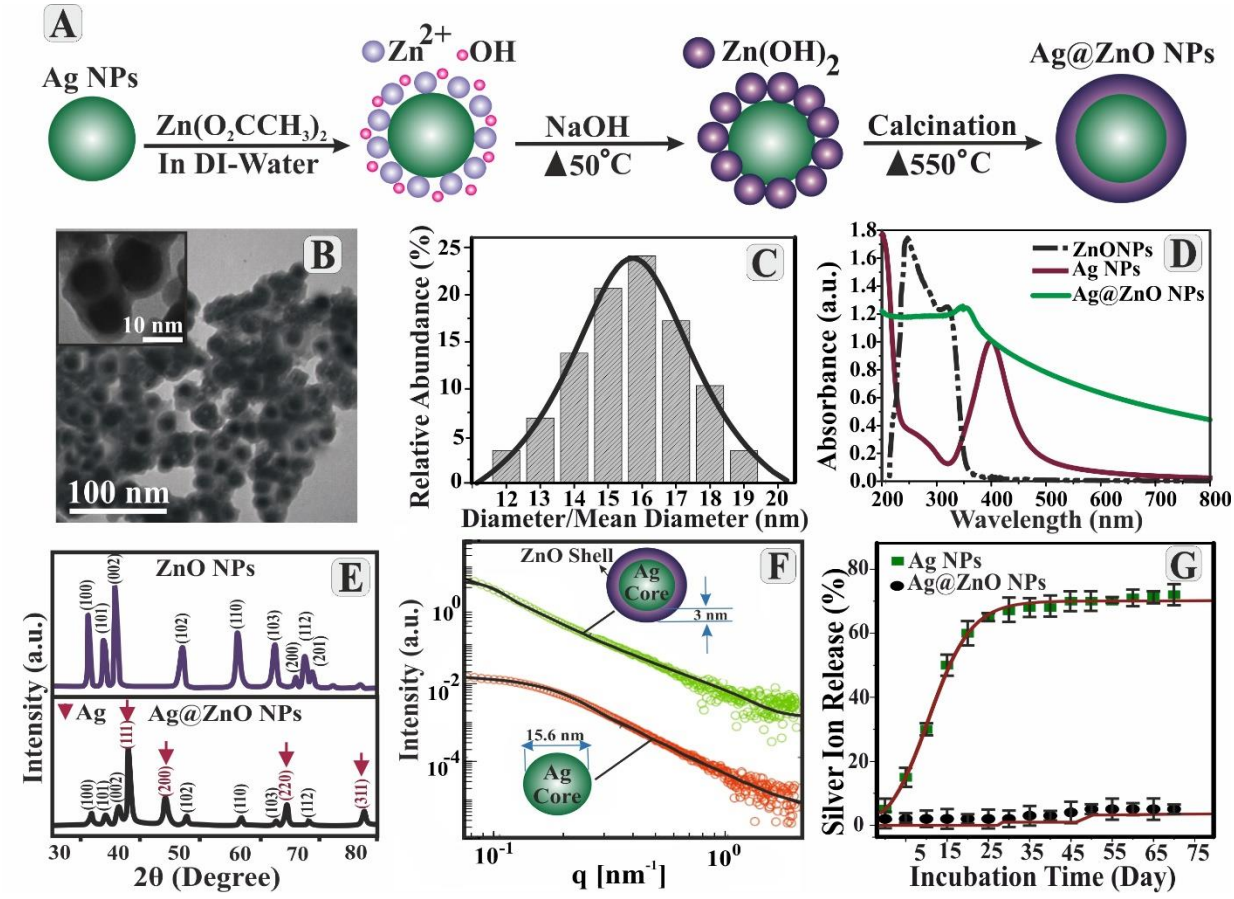

Figure 2. Schematic illustration of Ag@ZnO NPs synthesis procedure (A). Transmission Electron micrograph (TEM) of Ag@ZnO NPs (B) and corresponding size distribution analysis (C). UV-Vis spectra of Ag NPs, ZnO NPs and Ag@ZnO NPs (D). X-ray diffraction Spectroscopy (XRD) of ZnO and Ag@ZnO NPs (E). The experimental small angle scattering from Ag nanoparticles and the Ag@ZnO core-shell nanoparticles (open circles) together with the corresponding simulated curves (solid lines). The polydispersity parameters of 0.6 and 1 with a Schultz distribution function were used for Ag NPs and Ag@ZnO NPs, respectively (F). ICP-MS results for Ag^+ ions release studies during 75 days, evaluated every 5 days in water solutions (G)

Uptake of Ag@ZnO NPs by Cells

Inverted confocal microscopy was applied to evaluate cellular uptake of Ag@ZnO NPs in MDA-MB231 and MRC-5 cells. Also, in order to confirm the presence of fluorescent dye on the surface of prepared RhB-labeled Ag@ZnO NPs, they were characterized by UV-Vis spectroscopy as well as zeta sizer. Results of zeta potential measurement showed that conjugation of RhB on the surface of Ag@ZnO NPs reduces electric potential of bare surface of the Ag@ZnO NPs (Figure 3B). Interaction between surface atoms and the dye can result in modification of surface charge, thereby changes the zeta potential [28].

Moreover, obtained results for UV-Vis absorbance spectra indicates that Rh-B is bonded to the surface of NPs (Figure 3C) [29]. The spectrum exhibits an excitonic absorption peak at about 320 nm for free Ag@ZnO NPs and a single peak for RhB dye at 580 nm. In case of RhB labeled Ag@ZnO NPs, both peaks of NP and dye are noticeable due to a successful attachment of dye to NPs [30]. Additionally, labeling of Ag@ZnO NPs by Rh-B causes a small red shift in absorption peak (350 nm) of Ag@ZnO NPs. Obtained results of confocal microscopy studies showed that Ag@ZnO NPs are taken up by the cells efficiently after 2 h incubation (Figure 3 D, E and S4). Results show that 94% of cancer cells have taken up substantial amounts of Ag@ZnO NPs after 2 h of incubation, while results of NPs uptake by healthy cells showed a 78% NP uptake (Figure S5), which is comparable to previous report for ZnO NPs [13]. The red fluorescence of internalized Rh-B in extra nuclear region of the treated cells, clearly illustrates that the Ag@ZnO NPs could be internalized into the cancer cells (Figure 3E). Recent studies have shown that ZnO NPs have high affinities to cancer cells [31]. Also, They have different cytotoxicity profiles due to different cell uptake and cytotoxicity pathways [32]. Considering size as only determinant factor for nanoparticle uptake, it could be suggested that the Ag@ZnO NPs have the best potent size for cancer cell's internalization which was reported about 50 nm [33].

The DLS study of Ag@ZnO NPs dispersed in cell media showed a mean diameter of 70 nm. Since, it has been reported that 120 nm NPs are taken up through clathrin-mediated endocytosis and 50-80 nm NPs are mainly internalized by caveoline mediated endocytosis, the synthesized NPs have potential to uptake by endocytosis [34].

In-Vitro Toxicity Evaluation of Ag@ZnO NPs on Breast Cancer Cells

Low cytotoxicity of nanoparticles on healthy cells is a main condition for their biomedical applications. Toxic effects of Ag NPs, ZnO NPs and Ag@ZnO NPs on healthy lung fibroblast (MRC-5) and breast cancer (MDA-MB231) were assessed by MTT and LDH assays in dark and under UV radiation (Figure 4 A, B).

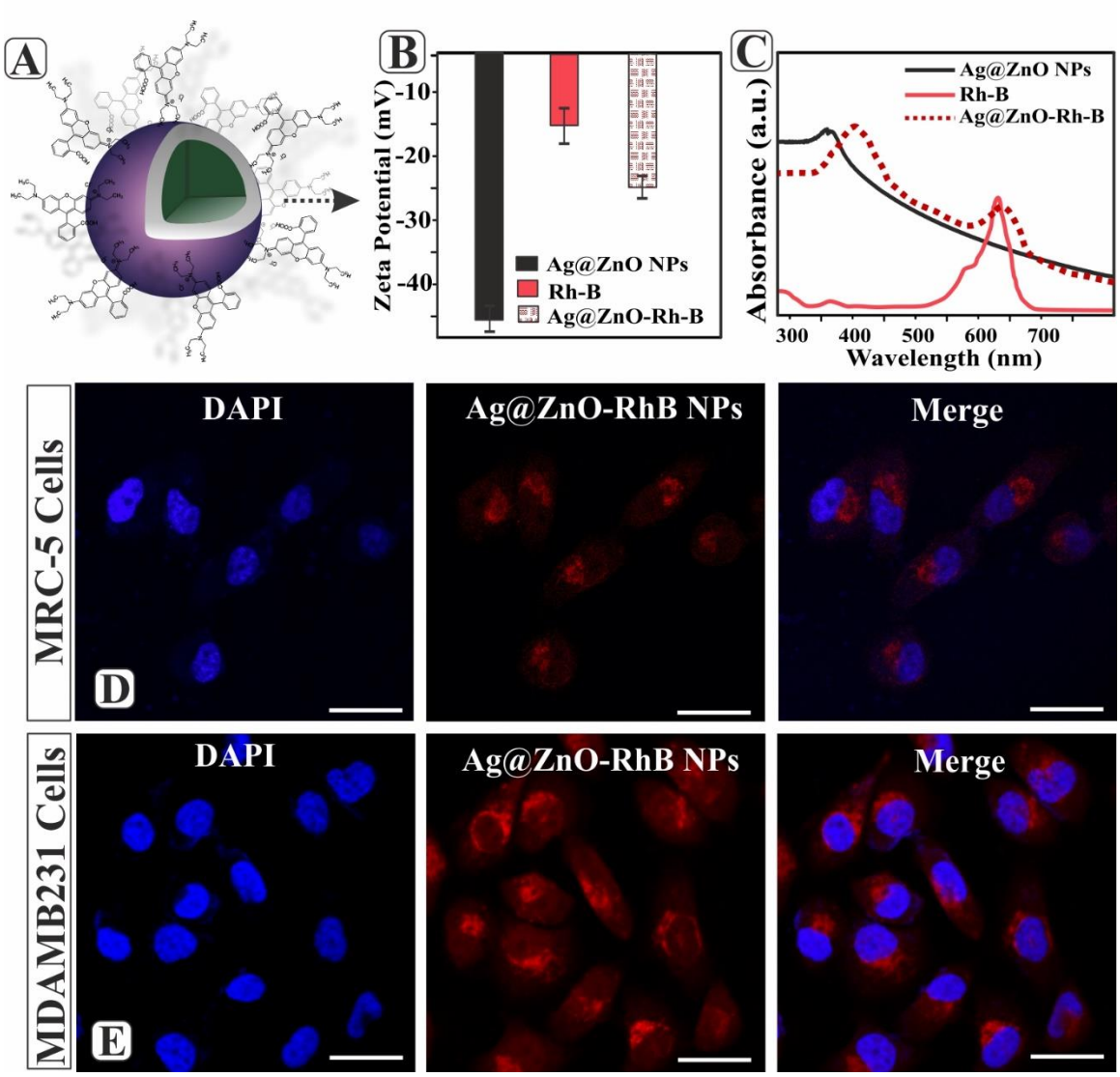

Figure 3. Schematic illustration of Rh-B conjugated Ag@ZnO NPs (A), Zeta potential evaluation of bare NPs and Rh-B conjugated NPs (B). UV-Vis spectra of Free Ag@ZnO NPs, Rh-B and Rh-B conjugated Ag@ZnO NPs (C), Representative corresponding laser confocal micrograph images of MRC-5 cells (D) and MDA-MB231 (E) incubated with Rh-B labelled Ag@ZnO NPs for 2 hours. Scale bar: 20 µm.

MTT Results in dark conditions revealed a dose-dependent cytotoxicity for all types of NPs. However, the cytotoxicity of Ag NPs is significantly higher than the other two groups. Cell lines treated with ZnO NPs and Ag@ZnO NPs, in dark condition, remained more than 70% viable at concentration 20 µg/ml (Figure 4A). The findings reveal that ZnO NPs and Ag@ZnO

NPs do not have any considerable cytotoxicity in cancerous and healthy cell lines in absence of excitation radiation. A previous research showed that naturally abundance of Zn^+ ions in the human body results in low toxicity of ZnO NPs which makes it a suitable nanoparticle in biomedical applications [35]. In Ag@ZnO NP, ZnO shell prevents the release of Ag^+ ions and decreases the cytotoxicity of Ag@ZnO NPs. A previous research showed that decrease of dissolution rate and amount of Ag^+ ions after coating with PVP resulted in decrease in cytotoxicity of Ag NPs [36]. Also, results of toxicity studies demonstrate that viability of healthy cells is generally more than the cancerous cells after treatment with NPs. The results indicate that healthy cells are able to tolerate mild oxidative stress due to higher antioxidant capacities[37,38].

Results of the MTT assays under UV radiation have also shown a concentration-dependence reduction in cell viability of NPs-treated cell lines (Figure 4B). From the details, ZnO NPs show concentration-dependent toxicity under UV radiation in cancer cells, although with less intense effect in comparison with Ag@ZnO NPs (Figure 4B). The cytotoxicity of Ag@ZnO NPs and ZnO NPs significantly increased (80% at 30 µg/ml concentration of Ag@ZnO and 65% for ZnO NPs) in presence of UV radiation exposure (Figure 4B). These excellent photocatalytic performances of ZnO NPs have been illustrated in previous observations (35, 36). Also, our results showed that Ag NPs under UV radiation have nearly similar toxic effects with dark condition on both cell lines. The research demonstrated that the main toxicity mechanisms of Ag NPs are due to release of Ag^+ ions which act as a Trojan horse, entering cells [39], a mechanism which is independent of radiation.

Internalization of NPs and consequent cytotoxicity are associated with release of LDH due to cell membrane disruption. Evaluation of LDH release showed that ZnO NPs and Ag@ZnO NPs cause~ 20% LDH release at the highest concentration (30 µg/ml) in dark conditions, while this value is about 80% for Ag NPs at same concentration (Figure 4C). This results is in

agreement with previous studies [40]. More importantly, treatment of cells with Ag@ZnO NPs under UV radiation significantly increases the release of LDH up to 97% in cancer cells compared with 60% for healthy cells at 30 µg/ml concentration, probably due to enhanced ROS generation in comparison with ZnO NPs. The results of LDH release indicate that antioxidant capacity of healthy cells are sufficient for protection against high amount of ROS [41]. Also, ZnO NPs have shown 65% LDH release in both cell lines, under UV radiation (Figure 4D). Furthermore, when comparing UV and dark condition, Ag NPs have similar toxic patterns. In total, results show that Ag@ZnO NPs are highly toxic under UV radiation, they are not considerably cytotoxic in dark conditions. Previous investigation has shown that coating of biogenic silver NPs by ZnO shell, has improved the anti-fungal properties of silver NPs without any significant toxicity on healthy cells [42]. Although, this report did not consider the effect of Ag@ZnO NPs as a photocatalyst nanomaterial, biocompatibility of synthesized NPs in dark condition was shown to improve. So, these properties could make them a perfect choice in targeted photodynamic therapy of cancer cells.

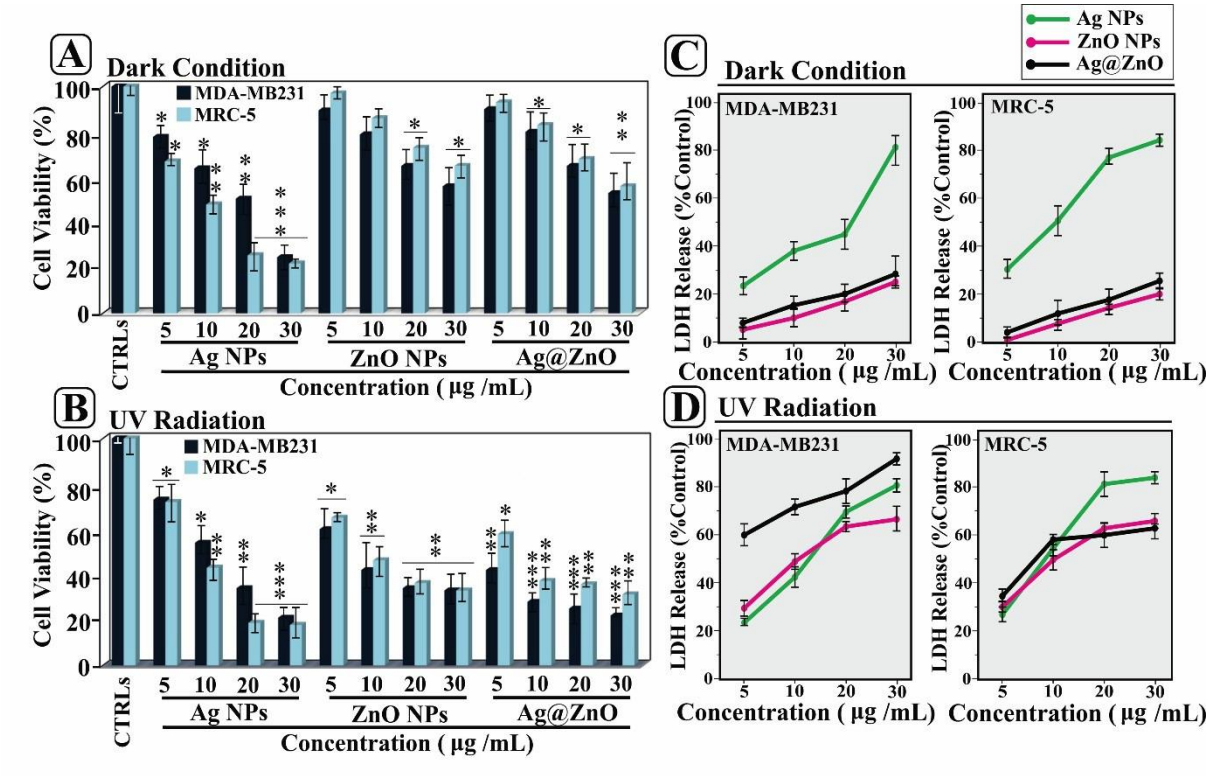

Figure 4. toxicity assessment of MRC-5 as healthy cells and MDA-MB231 as cancerous cells after treatment with different concentrations of Ag NPs, ZnO NPs and Ag@ZnO NPs in dark condition and under UV radiation. MTT assays (A, B), LDH Assays (C, D). All data were compared with control and the line means they are same significance.

Intracellular ROS-Dependent Cytotoxicity of Ag@ZnO NPs

Ag@ZnO NPs have a high potential to generate radicals due to direct contact of ZnO and Ag which results in interfacial processes of charge transfer when radiated by an external UV. Increased photocatalytic activity of Ag@ZnO NPs has previously been reported as solar photocatalytic disinfection process [21, 43]. Also, reports showed that induction of high amount of ROS, could remarkably overwhelm the antioxidant capacity of the cells and cause cell death [44].

So, inspired by previous works, in this research, ROS generation was measured by neutralization of DPPH as a stable radical. Results of DPPH assay showed that ZnO NPs and Ag@ZnO NPs generate high amount of ROS in a concentration dependent manner after exposure to UV radiation. Figure 5A shows that ZnO and Ag@ZnO NPs generate different amounts of ROS under UV radiation as discussed before. This consequence is particularly more obvious for Ag@ZnO NPs due to a higher photocatalytic activity. Previous reports have shown that ZnO NPs can produce ROS after stimulation by UV light [45]. Even though Ag NPs provided a strong toxicity profile in dark and under UV radiation on healthy and cancer cells, their ROS generation are less than the other NPs. This confirms that the main toxicity mechanism of Ag NPs is not ROS generation, but most probably release of Ag^+ ions [46]. Moreover, the high toxicity of Ag@ZnO NPs under UV radiation is dependent on ROS generation while these NPs are not toxic for cells in dark condition. Ag@ZnO NPs are able to generate free radicals during interaction with cellular components (*e.g.,* mitochondrial damage, Bax/Bcl2 modulation, caspases activation and apoptosis) [47]. The produced radicals can oxidize or reduce the DNA,

lipids and proteins and other important biological components, resulting in substantial oxidative damages to the cell. In this regard, flow cytometry was employed to evaluate different types of intracellular radicals for synthesized NPs under UV radiation (Figure 5B, C). The results of intracellular ROS in ZnO NPs and Ag@ZnO NPs-treated cells under UV radiation demonstrated an increase in fluorescence intensity of DCF and HE as markers of H_2O_2 and O_2 radicals in comparison with dark conditions (Figure 5B). From the details, Ag@ZnO NPs generated higher levels of H_2O_2 radicals associated with permanent photoactive holes on the surface [48]. These holes form spatially indirect excitons in the interface of Ag/ZnO which transfer to surface of NPs after UV excitation and result in a high amount of electron capture from environmental molecules and consequent H_2O_2 [49]. Ag@ZnO NPs has been reported as a high photocatalyst nanomaterial in catalysis applications and electronic procedures [15, 19]. Moreover, obtained results for ROS generation in dark condition (Figure 5B and S6), show no significant radical production for ZnO NPs and Ag@ZnO NPs-treated cells in comparison with untreated ones. Also, the estimated results for ROS generation suggest that Ag NPs induce medium levels of H_2O_2 and O_2 radicals in comparison with ZnO NPs and Ag@ZnO NPs. Furthermore, Ag@ZnO NPs-mediated intracellular ROS generation was determined by DCF fluorescence microscopy assay in MDA-MB 231 and MRC-5 cells (Figure 5C). The ROS-generation capability of Ag@ZnO NPs may lead to various pathways in cells which results in mutations and oxidative damage of cells[50-51]. Also, researcher reported that ZnO NPs induce oxidative stress, with significant formation of reactive oxygen species (ROS) inside the cells which trigger DNA damage and eventually result in cell death[52].

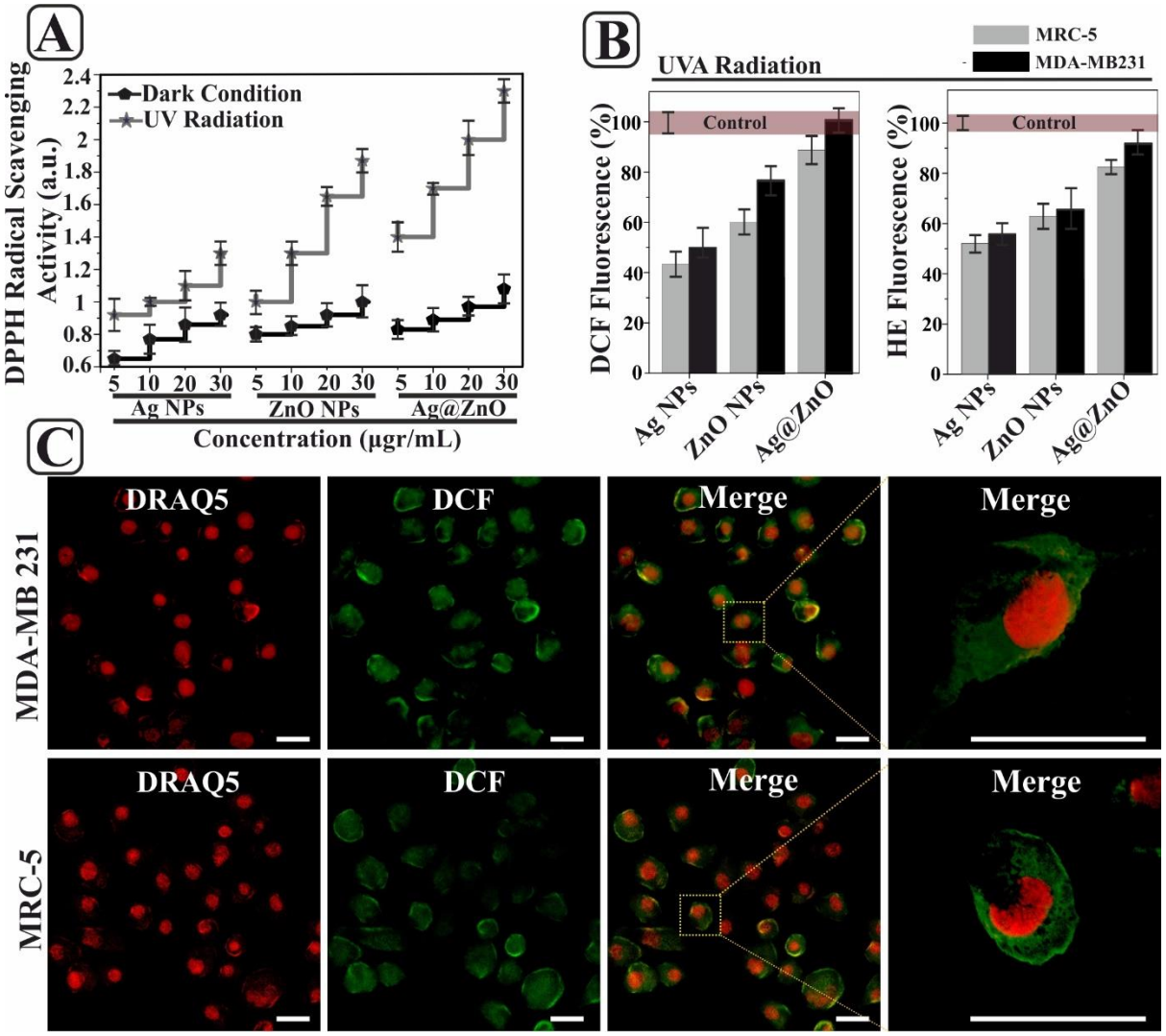

Figure 5. ROS generation ability of NPs in solution assessed with DPPH (A), Representative flow cytometry marker (B) for Ag NPs, ZnO NPs and Ag@ZnO NPs treated MDA-MB231 cells in dark condition and under UV radiation. Positive DCF fluorescence represents intracellular H_2O_2 and positive HE fluorescence represents intracellular $O_2^{\cdot}$. Representative microphotographs shows confocal study of intracellular ROS generation of Ag@ZnO NPs after UV radiation measured by DCF fluorescent in MDA-MB231 and MRC-5 Cells (C), Scale bar: 10 µm.

Glutathione reductase and superoxide dismutase are recognized as the most important cellular antioxidant enzymes in modulation, regulation and maintenance of cellular oxidative stress response as well as redox homoeostasis [53]. Hence, to investigate the potential role of oxidative stress, activity of the mentioned enzymes was monitored after treating cells with different concentrations of Ag NPs, ZnO NPs and Ag@ZnO NPs, in dark condition and under UV

radiation (Figure 6). Although, ZnO NPs and Ag@ZnO NPs in dark condition did not show any significant effect on increase of cellular antioxidant enzymes, Ag NPs significantly increased the amount of glutathione reductase as well as superoxide dismutase enzymes (Figure 6 A, B). Increase in enzymes activity is due to intracellular ROS generation of Ag NPs in dark condition as shown by flow cytometry results. Previous reports showed that treatment of rat liver cells with Ag NPs reduced glutathione levels, and raised ROS production, representing effect of metal NPs on respiratory chain. Also, generated ROS in presence of Ag NPs causes metabolic disturbances and toxicological consequences [54]. Subsequently, increase in oxidative stress levels results in enhancement of glutathione reductase and superoxide dismutase. After UV exposure to Ag@ZnO NPs, increased levels of superoxide dismutase (10-fold) and glutathione reductase (2-fold) in comparison with controls were observed. Generated oxidative stress by Ag@ZnO NPs under UV radiation as a mechanism of toxicity results in shift of overall redox balance to oxidation which leads to functional damage of cells [55] (Figure 6C).

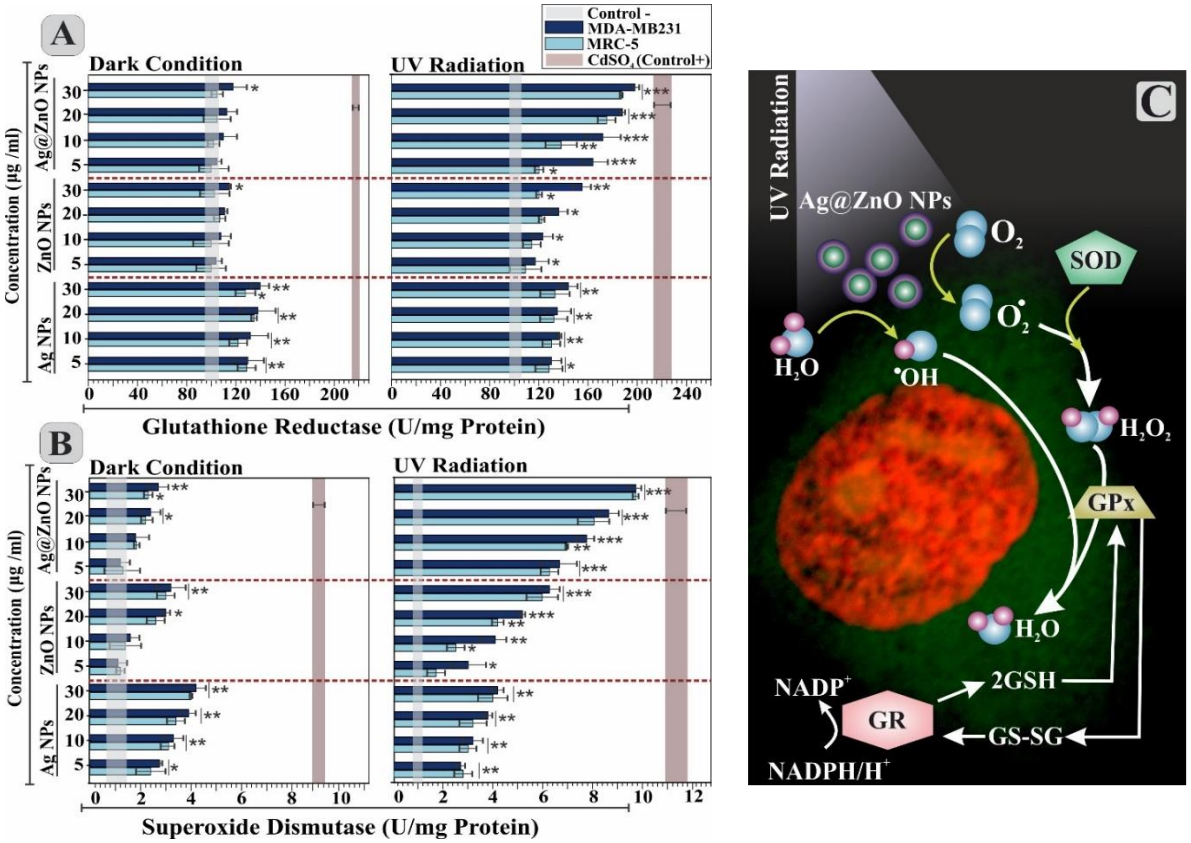

Figure 6. Antioxidant response of NPs–treated MDA-MB231 and MRC-5 cells in dark condition and under UV radiation, concentration of Gluthation reductase (A) and Superoxide dismutase (B) after treatment. (C) Schematic represents the cell's oxidative stress responses initiate by superoxide dismutase (SOD), glutathion reductase (GR) and glutathion peroxidase (GPx) in cells after treatment with Ag@ZnO NPs under UV radiation. The background shows the interacellular DCF green fluorescence as an indicator of ROS generation along with red colored MD-MB 231 nucleus after treatment with Ag@ZnO NPs which were captured by confocal microscopy.

Distinct Cellular Fates (Apoptosis and Related-Enzymatic Cascade)

To investigate mechanism of MDA-MB231 cell death induced by Ag@ZnO NPs, AnnexinV-PI assay was used for different concentrations. Obtained results for highest concentration of Ag@ZnO NPs-treated MDA-MB231 cells in dark condition showed 17.9% apoptosis and 5.1% necrosis which is consistent with cytotoxicity assays (Figure 7A). The results showed 20% cell death during treatment in dark condition. However, Results of UV treatment demonstrated that the main cause of cell death is apoptosis, about 31% of the cells were positive for necrosis/late apoptosis (Detailed in Figure S7). The enhanced concentration-dependent apoptosis of Ag@ZnO NPs indicates an exclusive role for ROS in killing cancerous cells[56]. Participation of ROS was shown by a strong positive association between ROS generation and early apoptosis (Figure S7). It has also been demonstrated that induced apoptosis by Ag NPs is mediated by oxidative stress in fibroblast, colon and lung cancer cell lines [55, 57].

Reports indicated that the oxidative stress is directly involved in DNA damage and causes intrinsic mitochondria-dependent apoptosis cascade. So, in this study, levels of key apoptotic cascade proteins (caspase 3, Bax/Bcl2, cytochrome C and P53) were measured in cells treated with NPs for 6 h. Among these, B-cell lymphoma 2 (Bcl-2) family controls outer mitochondrial membrane permeabilization and can apply pro-apoptotic (bax, bad, bak) effects by activation of an inner mitochondrial permeability transition pore[58-59]. Obtained results of Bax/Bcl2 studies showed no significant difference in enhancement of Bax/Bcl2 for cells treated with ZnO NPs

and Ag@ZnO NPs in dark condition, whereas Ag NPs enhanced Bax expression and decreased bcl2 (Figure 7B). The changes after Ag treatment may occur due to either release of Ag^+ ions or ROS generation in dark condition. Moreover, the results for MDA-MB231 cells after treatment with Ag@ZnO NPs under UV radiation showed modulation of Bax and Bcl2 protein levels with a significant increase in Bax expression and a parallel/corresponding decrease in Bcl2. These Bcl2 proteins play important role in mediated apoptosis by mitochondrial pathway which results in release of activated pro-apoptotic factors by caspase cascade [47].

Clearly, most of the chemotherapeutic drugs trigger the apoptosis through activation of p53 pathway. So, in this work, the effect of Ag@ZnO NP on p53 protein expression was determined using the enzyme-linked assay method. Herein, an up-regulation of p53 (2.5 folds) was observed at highest conncentration of Ag@ZnO NPs under UV radiation (Figure 7C). Results showed a significant difference in p53 expression between controls and cells treated with 20 and 30 μg/ml of Ag@ZnO NPs under UV radiation. Although, ZnO NPs and Ag@ZnO NPs did not show any significant increase in p53 in dark condition, Ag NPs showed increase in p53 amount in both dark and UV radiation. It has already been described that Bax protein is up-regulated by p53 protein [57]. Since an enhancement in Bax expression in cells treated with Ag@ZnO NP was observed, the role of p53 in up-regulation of Bax can be confirmed. Moreover, insertion of Bax into the mitochondrial membrane feasibly results in p53-mediated apoptosis [60]. Similar results showed that p53 plays an important role in Ag NP-induced apoptosis as a conseguence of interacellular ROS generation [61]. After treatment of MDA-MB231 cells with Ag@ZnO NPs under UV radiation, protein expression of cell cycle checkpoint p53 and pro-apoptotic bax were up-regulated, while expression of Bcl-2 as an anti-apoptotic gene was down-regulated, in comparison with control groups [59].

Furthermore, release of cytochrome C is an improtant marker for mitochondria-mediated apoptosis. MDA-MB231 cells treated with Ag@ZnO NPs, demonstrated an increase in release

of cytochrome C release in a concentration-dependent manner under UV radiation. The results for ZnO NPs and Ag@ZnO NPs-treated cells in dark condition have not shown any significant cytochrome release, wherese Ag NPs caused significant enhancement in release of cytochrom C in dark condition as well as UV radiation (Figure 7D). Also, leakage of cytochrome C from the mitochondria into the cytoplasm, triggers ROS pruduction and depletion of cellular glutathione which are related to apoptosis. Cytochrome C binds to apoptosis protease activating factor-1 (Apaf-1) which results in assembly of an apoptosome compound. The apoptosome could activate caspase-3, which cleaves substrates of aspartate residues and consequently leads to activation of proteolytics as an event in apoptosis [62].

Moreover, caspase3 is activated during apoptosis which is known as a vital protein in initiation/ execution of apoptosis. ROS is another factor that triggers the apoptotic cascade [63]. In this context, activation of caspase-3 is considered as a point with no return in apoptosis pathway [64]. Caspase-3 activation causes cleavage of ICAD (inhibitor of caspase-activated DNAse) and translocation of CAD (caspase-activated DNAse) to the nucleus which results in DNA fragmentation [55]. DNA cleavage is the most noticeable event in early stages of apoptosis [65]. Also, caspase-3 is identified as ultimate responsible factor for apoptosome formation, in caspase-dependent pathway of apoptosis. The results showed higher activity (2.5 fold) of caspase-3 in cells treated with 30 µg/ml of Ag@ZnO NPs under UV radiation, in comparison with controls (Figure 7E).

Our apoptotic data supported the ROS-induced cytotoxicity of Ag@ZnO NPs which causes higher apoptotic response than Ag NPs and ZnO NPs under UV radiation. Previous reports explained that toxicity of ZnO NPs is due to dissolution of the particles into Zn^{2+} ions [66]. However, some investigations state that the amount of released Zn^{2+} ions in aqueous medium, are insufficient to stimulate cytotoxicity in human cells[67]. The schematic in Figure 7F represents the involved proteins in apoptotic pathway which starts with Ag@ZnO NPs as a

consequence of ROS generation. Furthermore, All experiments were performed for healthy cells as well, and showed that the importance of the protein expression after oxidative stress is to some extent similar in healthy and cancerous cells.

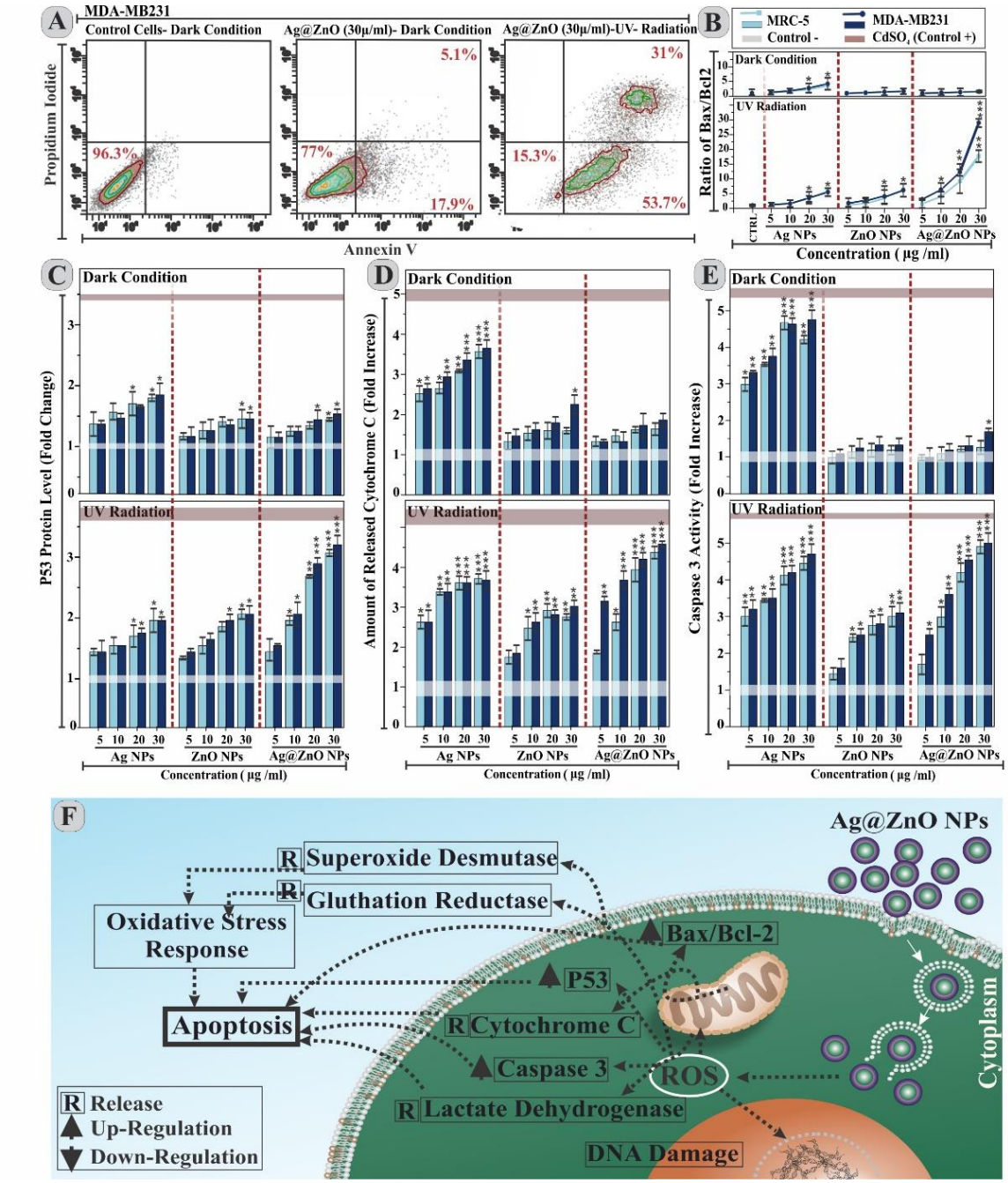

Figure 7. Flowcytometry results of control in comparison with Ag@ZnO NPs treated cells in dark condition and under UV radiation (A). Release of Bax/Bcl2 in Ag@ZnO NPs treated cells (B). Evaluation of protein changes of cells after treatment with Ag@ZnO NPs; P53 (C), Release of Cytchrome C (D) and caspase 3 activity (E) in dark condition and under UV radiation. Schematic represents the apoptosis mechanisems which triggers by Ag@ZnO NPs.

The uptaken NPs, generate ROS after excitation with UV radiation which are triggered activation of p53 protein. In turn, p53, a known activator of pro-apoptotic genes, activates bax and decrease the amount of bcl2. These proteins cause mitochondrial membrane leakage subsequence cytochrome C release, which activates caspase-3 in the apoptotic cascade. Eventually, caspase-3 induces DNA fragmentation with cleavage of nuclear membrane and causes apoptosis (F).

CT/ Optical dual contrast enhancement of Ag@ZnO NPs

To evaluate possible diagnostic application of Ag@ZnO NPs, the synthesized NPs were examined as CT/optical imaging contrast agents, followed by photo luminescence (PL) spectra evaluation.

In this regard, capability of Ag@ZnO NPs as CT contrast agents were examined by applying a 16 slice clinical CT imaging system. In order to evaluate the efficiency of synthesized NPs as CT contrast agent, their X-ray attenuation ability was compared with Visipaque®, the widely used CT contrast agent in clinical imaging. Obtained results showed an enhancement in contrast and brightness of CT images for Ag NPs and Ag@ZnO NPs, in comparison with water as control negative (Figure 8). Moreover, Ag@ZnO NPs showed an extensive enhancement in image contrast at concentrations of 0.08 mM compared with conventionally used contrast agent (i.e. Visipaque® at 225 mM concentration). Therefore, it is arguable that ZnO NPs protection layer in Ag@ZnO NPs, makes the NPs stable and safe contrast agents for CT tomography. Additionally, core structure of Ag@ZnO NPs makes them potential agents for X-ray computed tomography with lower concentration, in comparison with iodine-based molecular CT contrast agents. The lower concentration could considerably reduce side effects of the contrast agents [68]. Previous reports have shown that high atomic number elements, like lanthanides doped in ZnO crystal [13], Gd-coated/conjugated Au NPs [69] , Ag NPs with different sizes [70] and Au-Fe alloy nanoparticles [71] could potentially enhance the contrast of CT images. Using high atomic number elements in structure of NPs, makes them capable of being traced in CT imaging at potentially safe concentrations.

Figure 8A shows the PL spectra of Ag@ZnO NPs in ambient temperature which comprises two emission bands in the UV/visible region with 325 nm excitation wavelength. Obtained graph shows an intense narrow emission peak in UV range centered at 380 nm for ZnO without any specific position changes after adding Ag NPs as core in Ag@ZnO NPs. Normally, this emission is assigned to the excitonic recombination in ZnO NPs [72]. Also, lower intensity emission band centered at 320 nm is related to exciton recombination of Ag and ZnO interfaces which comes from some border traps of radiative defects between Ag and ZnO [73]. After addition of ZnO as shell, PL intensity in ultraviolet is practically quenched due to the charge transfer from ZnO to Ag, which provides perfect evidence that the semiconductor-metal contact increases the photo activity of core/shell structure. In addition, The Ag@ZnO NPs showed a wider peak in the visible region, centered at 580 nm (*i.e.* 520-650) with lower intensity in comparison with pure ZnO NPs. These multicomponent wide visible emission spectra in ZnO are related to some intrinsic and extrinsic defects which encompass the orange/red fluorescent region [74].

In this regard, the results for optical images demonstrated an orange, red fluorescent color for ZnO NPs and Ag@ZnO NPs, respectively. The fluorescent color of images converted brighter, corresponding to the rise in concentrations. Even though these NPs are not applicable for conventional confocal study, due to excitation limitation of lasers, obtained results showed that Ag@ZnO NPs could serve as effective optical imaging contrast agents. literature shows that the non-centrosymmetric structure of ZnO NPs can be used as non-resonant/ non-linear optical probe for biomedical applications [75]. Also, previous reports demonstrate the application of rare earth element-doped nanocrystals as fluorescent probes for cathodoluminescence electron microscopy bio-imaging [76]. Overly, these specific structures consist of high atomic number elements in core as well as photoactive ZnO as shell, make the NPs capable to be traced in CT/optical imaging at safe concentrations.

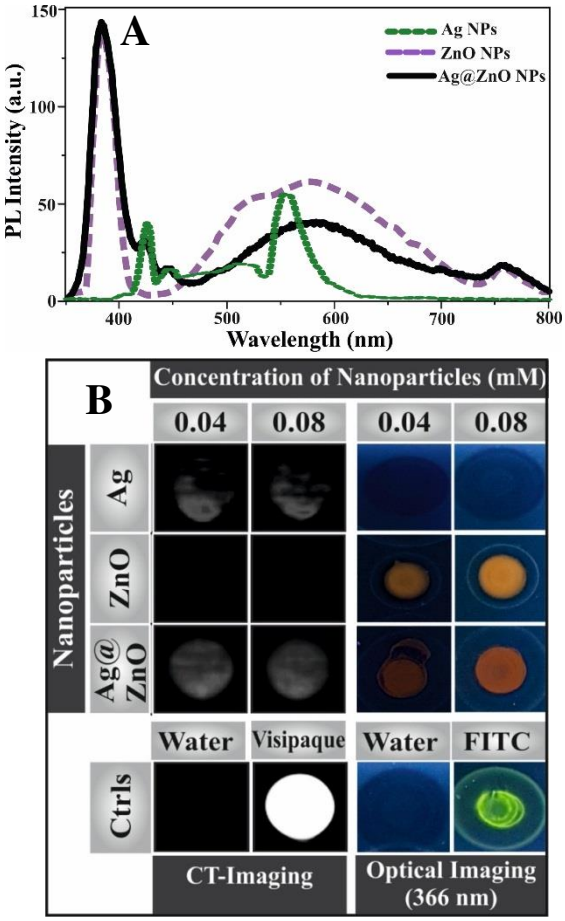

Figure 8. PL luminescence spectrum of Ag, ZnO and Ag@ZnO NPs (A). 16 slice clinical-CT tomograph of synthesized NPs with different concentrations in comparison with water and Visipaque®. Signal strength is indicated by the brightness of the images (B, left), optical images of NPs in 325 nm UV excitation in comparison with FITC as control positive flourescent.

Conclusion

We found that Ag@ZnO NPs as novel nanocomposite structure, improve the characteristic photoactivity of ZnO NPs under UV radiation on treatment of human breast cancer cells while represent minimum toxicity in dark conditions. The improved photocatalytic activity of Ag@ZnO NPs is related to charge transfer in metal/semiconductor interfaces. Moreover,

enhanced ROS generation and photocatalytic activity of Ag@ZnO NPs, trigger apoptosis related pathway in breast cancer cells through activation of tumor suppressor gene p53 and along with cytochrome C and caspase-3 proteins. Also, Increase in Bax/Bcl2 ratio suggests that Ag@ZnO NPs prompt apoptosis through mitochondrial pathway. Furthermore, Ag@ZnO NPs showed the capability to be assisted in multimodal detection by CT/optical imaging. Based on results, Ag@ZnO NPs are potentially applicable for simultaneous imaging and therapy as targeted photosensitizer in photodynamic therapy.

Conflicts of Interest

There are no conflicts to declare.

Acknowledgment

This study was supported by Tehran University of Medical Science (TUMS) through the grant number 97-01-87-37512.

Supporting Information

Methods and Materials, TEM micrographs, DLS studies in water and DMEM, XRD pattern of Ag@$Zn(OH)_2$, optical microscopy images of Ag@ZnO NPs uptake, quantitative uptake histogram, Flowcytometry of interacellular ROS with DCFDA and DHE in dark condition and UV radiation, detailed amount of apoptosis/necrosis.

References

1. Comfort, K. K.; Braydich-Stolle, L. K.; Maurer, E. I.; Hussain, S. M., Less is More: Long-Term in vitro Exposure to Low Levels of Silver Nanoparticles Provides New Insights for Nanomaterial Evaluation. *ACS nano* **2014,** *8* (4), 3260-3271.
2. Huang, X.; El-Sayed, I. H.; Qian, W.; El-Sayed, M. A., Cancer Cell Imaging and Photothermal Therapy in the Near-infrared Region by Using Gold Nanorods. *Journal of the American Chemical Society* **2006,** *128* (6), 2115-2120.
3. Najafi-taher, R.; Ghaemi, B.; Kharazi, S.; Rasoulikoohi, S.; Amani, A., Promising Antibacterial Effects of Silver Nanoparticle-Loaded Tea Tree Oil Nanoemulsion: a Synergistic Combination Against Resistance Threat. *AAPS PharmSciTech* **2017**, 1-8.
4. Jiang, W.; Kim, B. Y.; Rutka, J. T.; Chan, W. C., Nanoparticle-Mediated Cellular Response is Size-Dependent. *Nature nanotechnology* **2008,** *3* (3), 145-150.
5. He, C.; Lu, K.; Liu, D.; Lin, W., Nanoscale Metal–Organic Frameworks for the Co-delivery of Cisplatin and Pooled siRNAs to Enhance Therapeutic Efficacy in Drug-resistant Ovarian Cancer Cells. *Journal of the American Chemical Society* **2014,** *136* (14), 5181-5184.
6. Macias-Montero, M.; Peláez, R. J.; Rico, V. J.; Saghi, Z.; Midgley, P.; Afonso, C. N.; González-Elipe, A. R.; Borras, A., Laser Treatment of Ag@ ZnO Nanorods as Long-life-span SERS Surfaces. *ACS applied materials & interfaces* **2015,** *7* (4), 2331-2339.
7. Liu, F.; Hou, Y.; Gao, S., Exchange-coupled Nanocomposites: Chemical Synthesis, Characterization and Applications. *Chemical Society Reviews* **2014,** *43* (23), 8098-8113.
8. Qi, J.; Dang, X.; Hammond, P. T.; Belcher, A. M., Highly Efficient Plasmon-enhanced Dye-sensitized Solar Cells Through Metal@ oxide Core–shell Nanostructure. *ACS nano* **2011,** *5* (9), 7108-7116.
9. Maj, T.; Wang, W.; Crespo, J.; Zhang, H.; Wang, W.; Wei, S.; Zhao, L.; Vatan, L.; Shao, I.; Szeliga, W., Oxidative Stress Controls Regulatory T cell Apoptosis and Suppressor Activity and PD-L1-blockade Resistance in Tumor. *Nature immunology* **2017,** *18* (12), 1332.
10. Hirakawa, T.; Kamat, P. V., Charge Separation and Catalytic Activity of Ag@ TiO2 Core− shell Composite Clusters Under UV− irradiation. *Journal of the American Chemical Society* **2005,** *127* (11), 3928-3934.
11. Gong, C.; Colombo, L.; Wallace, R. M.; Cho, K., The Unusual Mechanism of Partial Fermi Level Pinning at Metal–MoS2 Interfaces. *Nano letters* **2014,** *14* (4), 1714-1720.
12. Li, P.; Wei, Z.; Wu, T.; Peng, Q.; Li, Y., Au− ZnO Hybrid Nanopyramids and Their Photocatalytic Properties. *Journal of the American Chemical Society* **2011,** *133* (15), 5660-5663.
13. Ghaemi, B.; Mashinchian, O.; Mousavi, T.; Karimi, R.; Kharrazi, S.; Amani, A., Harnessing the Cancer Radiation Therapy by Lanthanide-doped Zinc Oxide Based Theranostic Nanoparticles. *ACS applied materials & interfaces* **2016,** *8* (5), 3123-3134.
14. Viswanatha, R.; Brovelli, S.; Pandey, A.; Crooker, S. A.; Klimov, V. I., Copper-doped Inverted Core/shell Nanocrystals with "Permanent" Optically Active Holes. *Nano letters* **2011,** *11* (11), 4753-4758.
15. Clavero, C., Plasmon-induced Hot-electron Generation at Nanoparticle/metal-oxide Interfaces for Photovoltaic and Photocatalytic Devices. *Nature Photonics* **2014,** *8* (2), 95-103.
16. Hirakawa, T.; Kamat, P. V., Charge Separation and Catalytic Activity of Ag@ TiO2 Core-shell Composite Clusters under UV-irradiation. *Journal of the American Chemical Society* **2005,** *127* (11), 3928-3934.
17. Hirakawa, T.; Kamat, P. V., Photoinduced Electron Storage and Surface Plasmon Modulation in Ag@ TiO2 Clusters. *Langmuir* **2004,** *20* (14), 5645-5647.
18. Zhai, H.; Wang, L.; Han, D.; Wang, H.; Wang, J.; Liu, X.; Lin, X.; Li, X.; Gao, M.; Yang, J., Facile One-step synthesis and Photoluminescence Properties of Ag–ZnO core–shell Structure. *Journal of Alloys and Compounds* **2014,** *600*, 146-150.

19. Chen, X.; Li, Y.; Pan, X.; Cortie, D.; Huang, X.; Yi, Z., Photocatalytic Oxidation of Methane Over Silver Decorated Zinc Oxide Nanocatalysts. *Nature communications* **2016,** *7*.
20. Encina, E. R.; Pérez, M. A.; Coronado, E. A., Synthesis of Ag@ ZnO Core–shell Hybrid Nanostructures: an Optical Approach to Reveal the Growth Mechanism. *Journal of nanoparticle research* **2013,** *15* (6), 1-12.
21. Liu, H.; Shao, G.; Zhao, J.; Zhang, Z.; Zhang, Y.; Liang, J.; Liu, X.; Jia, H.; Xu, B., Worm-like Ag/ZnO Core–shell Heterostructural Composites: Fabrication, Characterization, and Photocatalysis. *The Journal of Physical Chemistry C* **2012,** *116* (30), 16182-16190.
22. Xiu, Z.-m.; Zhang, Q.-b.; Puppala, H. L.; Colvin, V. L.; Alvarez, P. J., Negligible Particle-specific Antibacterial Activity of Silver Nanoparticles. *Nano letters* **2012,** *12* (8), 4271-4275.
23. Verano-Braga, T.; Miethling-Graff, R.; Wojdyla, K.; Rogowska-Wrzesinska, A.; Brewer, J. R.; Erdmann, H.; Kjeldsen, F., Insights into the Cellular Response Triggered by Silver Nanoparticles Using Quantitative Proteomics. *ACS nano* **2014,** *8* (3), 2161-2175.
24. Richter, A. P.; Brown, J. S.; Bharti, B.; Wang, A.; Gangwal, S.; Houck, K.; Hubal, E. A. C.; Paunov, V. N.; Stoyanov, S. D.; Velev, O. D., An Environmentally Benign Antimicrobial Nanoparticle Based on a Silver-infused Lignin Core. *Nature nanotechnology* **2015,** *10* (9), 817-823.
25. Wang, L.; Li, J.; Pan, J.; Jiang, X.; Ji, Y.; Li, Y.; Qu, Y.; Zhao, Y.; Wu, X.; Chen, C., Revealing the Binding Structure of the Protein Corona on Gold Nanorods Using Synchrotron Radiation-based Techniques: Understanding the Reduced Damage in cell Membranes. *Journal of the American Chemical Society* **2013,** *135* (46), 17359-17368.
26. Navarro, E.; Wagner, B.; Odzak, N.; Sigg, L.; Behra, R., Effects of Differently Coated Silver Nanoparticles on the Photosynthesis of Chlamydomonas Reinhardtii. *Environmental science & technology* **2015,** *49* (13), 8041-8047.
27. Guo, D.; Zhu, L.; Huang, Z.; Zhou, H.; Ge, Y.; Ma, W.; Wu, J.; Zhang, X.; Zhou, X.; Zhang, Y., Anti-Leukemia Activity of PVP-coated Silver Nanoparticles via Generation of Reactive Oxygen Species and Release of Silver Ions. *Biomaterials* **2013,** *34* (32), 7884-7894.
28. Kitchin, J. R.; Nørskov, J. K.; Barteau, M. A.; Chen, J., Role of Strain and Ligand Effects in the Modification of the Electronic and Chemical Properties of Bimetallic Surfaces. *Physical review letters* **2004,** *93* (15), 156801.
29. Luk, B. T.; Zhang, L., Current Advances in Polymer-Based Nanotheranostics for Cancer Treatment and Diagnosis. *ACS applied materials & interfaces* **2014,** *6* (24), 21859-21873.
30. Talam, S.; Karumuri, S. R.; Gunnam, N., Synthesis, Characterization, and Spectroscopic Properties of ZnO Nanoparticles. *ISRN Nanotechnology* **2012,** *2012*.
31. Hanley, C.; Layne, J.; Punnoose, A.; Reddy, K.; Coombs, I.; Coombs, A.; Feris, K.; Wingett, D., Preferential Killing of Cancer Cells and Activated Human T Cells Using ZnO Nanoparticles. *Nanotechnology* **2008,** *19* (29), 295103.
32. Premanathan, M.; Karthikeyan, K.; Jeyasubramanian, K.; Manivannan, G., Selective Toxicity of ZnO Nanoparticles Toward Gram-positive Bacteria and Cancer Cells by Apoptosis Through Lipid Peroxidation. *Nanomedicine: Nanotechnology, Biology and Medicine* **2011,** *7* (2), 184-192.
33. Chithrani, B. D.; Chan, W. C., Elucidating the Mechanism of Cellular Uptake and Removal of Protein-coated Gold Nanoparticles of Different Sizes and Shapes. *Nano letters* **2007,** *7* (6), 1542-1550.
34. Rauch, J.; Kolch, W.; Laurent, S.; Mahmoudi, M., Big Signals from Small Particles: Regulation of Cell Signaling Pathways by Nanoparticles. *Chemical reviews* **2013,** *113* (5), 3391-3406.
35. Gulia, S.; Kakkar, R., ZnO Quantum Dots for Biomedical Applications. *Adv. Mat. Lett* **2013,** *4* (12), 876-887.
36. Yang, X.; Gondikas, A. P.; Marinakos, S. M.; Auffan, M.; Liu, J.; Hsu-Kim, H.; Meyer, J. N., Mechanism of Silver Nanoparticle Toxicity is Dependent on Dissolved Silver and Surface Coating in Caenorhabditis Elegans. *Environmental science & technology* **2011,** *46* (2), 1119-1127.
37. Alkilany, A. M.; Mahmoud, N. N.; Hashemi, F.; Hajipour, M. J.; Farvadi, F.; Mahmoudi, M., Misinterpretation in Nanotoxicology: A Personal Perspective. *Chemical research in toxicology* **2016,** *29* (6), 943-948.

38. He, T.; Peterson, T. E.; Holmuhamedov, E. L.; Terzic, A.; Caplice, N. M.; Oberley, L. W.; Katusic, Z. S., Human Endothelial Progenitor Cells Tolerate Oxidative Stress due to Intrinsically High Expression of Manganese Superoxide Dismutase. *Arteriosclerosis, thrombosis, and vascular biology* **2004,** *24* (11), 2021-2027.
39. Hsiao, I.-L.; Hsieh, Y.-K.; Wang, C.-F.; Chen, I.-C.; Huang, Y.-J., Trojan-horse Mechanism in the Cellular Uptake of Silver Nanoparticles Verified by Direct Intra-and Extracellular Silver Speciation Analysis. *Environmental science & technology* **2015,** *49* (6), 3813-3821.
40. Teodoro, J. S.; Silva, R.; Varela, A. T.; Duarte, F. V.; Rolo, A. P.; Hussain, S.; Palmeira, C. M., Low-dose, Subchronic Exposure to Silver Nanoparticles Causes Mitochondrial Alterations in Sprague–Dawley Rats. *Nanomedicine* **2016,** *11* (11), 1359-1375.
41. Nagano, O.; Okazaki, S.; Saya, H., Redox Regulation in Stem-like Cancer Cells by CD44 Variant Isoforms. *Oncogene* **2013,** *32* (44), 5191-5198.
42. Das, B.; Khan, M. I.; Jayabalan, R.; Behera, S. K.; Yun, S.-I.; Tripathy, S. K.; Mishra, A., Understanding the Antifungal Mechanism of Ag@ ZnO Core-shell Nanocomposites against Candida krusei. *Scientific reports* **2016,** *6*, 36403.
43. Das, S.; Sinha, S.; Suar, M.; Yun, S.-I.; Mishra, A.; Tripathy, S. K., Solar-photocatalytic Disinfection of Vibrio Cholerae by Using Ag@ ZnO Core–shell Structure Nanocomposites. *Journal of Photochemistry and Photobiology B: Biology* **2015,** *142*, 68-76.
44. Xia, T.; Kovochich, M.; Brant, J.; Hotze, M.; Sempf, J.; Oberley, T.; Sioutas, C.; Yeh, J. I.; Wiesner, M. R.; Nel, A. E., Comparison of the Abilities of Ambient and Manufactured Nanoparticles to Induce Cellular Toxicity According to an Oxidative Stress Paradigm. *Nano Lett.* **2006,** *6* (8), 1794-1807.
45. Guo, D.; Wu, C.; Jiang, H.; Li, Q.; Wang, X.; Chen, B., Synergistic Cytotoxic Effect of Different Sized ZnO Nanoparticles and Daunorubicin Against Leukemia Cancer Cells Under UV Irradiation. *J. Photochem. Photobiol. B* **2008,** *93* (3), 119-126.
46. Osborne, O. J.; Lin, S.; Chang, C. H.; Ji, Z.; Yu, X.; Wang, X.; Lin, S.; Xia, T.; Nel, A. E., Organ-Specific and Size-Dependent Ag Nanoparticle Toxicity in Gills and Intestines of Adult Zebrafish. *ACS nano* **2015,** *9* (10), 9573-9584.
47. Sharma, V.; Anderson, D.; Dhawan, A., Zinc Oxide Nanoparticles Induce Oxidative DNA Damage and ROS-triggered Mitochondria Mediated Apoptosis in Human Liver Cells (HepG2). *Apoptosis* **2012,** *17* (8), 852-870.
48. Wen, Z.; Li, C.; Wu, D.; Li, A.; Ming, N., Ferroelectric-Field-Effect-Enhanced Electroresistance in Metal/Ferroelectric/Semiconductor Tunnel Junctions. *Nature materials* **2013,** *12* (7), 617.
49. Wu, K.; Chen, J.; McBride, J. R.; Lian, T., Efficient Hot-electron Transfer by a plasmon-induced interfacial charge-transfer transition. *Science* **2015,** *349* (6248), 632-635.
50. Serpooshan, V.; Sheibani, S.; Pushparaj, P.; Wojcik, M.; Jang, A. Y.; Santoso, M. R.; Jang, J. H.; Huang, H.; Safavi-Sohi, R.; Haghjoo, N., Effect of Cell Sex on Uptake of Nanoparticles: The Overlooked Factor at the Nanobio Interface. *ACS nano* **2018**.
51. Lucky, S. S.; Muhammad Idris, N.; Li, Z.; Huang, K.; Soo, K. C.; Zhang, Y., Titania Coated Upconversion Nanoparticles for Near-infrared Light Triggered Photodynamic Therapy. *ACS nano* **2015,** *9* (1), 191-205.
52. Chakraborti, S.; Chakraborty, S.; Saha, S.; Manna, A.; Banerjee, S.; Adhikary, A.; Sarwar, S.; Hazra, T. K.; Das, T.; Chakrabarti, P., PEG-functionalized Zinc Oxide Nanoparticles Induce Apoptosis in Breast Cancer Cells Through Reactive Oxygen Species-Dependent Impairment of DNA Damage Repair Enzyme NEIL2. *Free Radical Biology and Medicine* **2017,** *103*, 35-47.
53. Couto, N.; Wood, J.; Barber, J., The Role of Glutathione Reductase and Related Enzymes on Cellular Redox Homoeostasis Network. *Free Radical Biology and Medicine* **2016,** *95*, 27-42.
54. AshaRani, P.; Low Kah Mun, G.; Hande, M. P.; Valiyaveettil, S., Cytotoxicity and Genotoxicity of Silver Nanoparticles in Human Cells. *ACS nano* **2008,** *3* (2), 279-290.
55. Arora, S.; Jain, J.; Rajwade, J.; Paknikar, K., Cellular Responses Induced by Silver Nanoparticles: In Vitro Studies. *Toxicology letters* **2008,** *179* (2), 93-100.

56. Mahmoudi, M., Debugging Nano–Bio Interfaces: Systematic Strategies to Accelerate Clinical Translation of Nanotechnologies. *Trends in biotechnology* **2018**.
57. Jeong, J.-K.; Gurunathan, S.; Kang, M.-H.; Han, J. W.; Das, J.; Choi, Y.-J.; Kwon, D.-N.; Cho, S.-G.; Park, C.; Seo, H. G., Hypoxia-mediated Autophagic Flux Inhibits Silver Nanoparticle-Triggered Apoptosis in Human Lung Cancer Cells. *Scientific reports* **2016,** *6*, 21688.
58. Xu, X.; Saw, P. E.; Tao, W.; Li, Y.; Ji, X.; Yu, M.; Mahmoudi, M.; Rasmussen, J.; Ayyash, D.; Zhou, Y., Tumor Microenvironment-Responsive Multistaged Nanoplatform for Systemic RNAi and Cancer Therapy. *Nano letters* **2017,** *17* (7), 4427-4435.
59. Czabotar, P. E.; Lessene, G.; Strasser, A.; Adams, J. M., Control of Apoptosis by the BCL-2 Protein Family: Implications for Physiology and Therapy. *Nature reviews. Molecular cell biology* **2014,** *15* (1), 49.
60. Akhtar, M. J.; Alhadlaq, H. A.; Alshamsan, A.; Khan, M. M.; Ahamed, M., Aluminum Doping Tunes Band Gap Energy Level as Well as Oxidative Stress-Mediated Cytotoxicity of ZnO Nanoparticles in MCF-7 cells. *Scientific reports* **2015,** *5*, 13876.
61. Zhu, B.; Li, Y.; Lin, Z.; Zhao, M.; Xu, T.; Wang, C.; Deng, N., Silver Nanoparticles Induce HePG-2 Cells Apoptosis Through ROS-mediated Signaling Pathways. *Nanoscale research letters* **2016,** *11* (1), 198.
62. Youle, R. J.; Strasser, A., The BCL-2 Protein Family: Opposing Activities that Mediate Cell Death. *Nature reviews. Molecular cell biology* **2008,** *9* (1), 47.
63. Green, D.; Kroemer, G., The Central Executioners of Apoptosis: Caspases or Mitochondria? *Trends in cell biology* **1998,** *8* (7), 267-271.
64. Wagener, F.; Dekker, D.; Berden, J.; Scharstuhl, A.; Van der Vlag, J., The Role of Reactive Oxygen Species in Apoptosis of the Diabetic Kidney. *Apoptosis* **2009,** *14* (12), 1451-1458.
65. Rogers, C.; Fernandes-Alnemri, T.; Mayes, L.; Alnemri, D.; Cingolani, G.; Alnemri, E. S., Cleavage of DFNA5 by Caspase-3 During Apoptosis Mediates Progression to Secondary Necrotic/Pyroptotic Cell Death. *Nature communications* **2017,** *8*, 14128.
66. Xia, T.; Zhao, Y.; Sager, T.; George, S.; Pokhrel, S.; Li, N.; Schoenfeld, D.; Meng, H.; Lin, S.; Wang, X., Decreased Dissolution of ZnO by Iron Doping Yields Nanoparticles With Reduced Toxicity in the Rodent Lung and Zebrafish Embryos. *ACS nano* **2011,** *5* (2), 1223-1235.
67. Moos, P. J.; Chung, K.; Woessner, D.; Honeggar, M.; Cutler, N. S.; Veranth, J. M., ZnO Particulate Matter Requires Cell Contact for Toxicity in Human Colon Cancer Cells. *Chemical research in toxicology* **2010,** *23* (4), 733-739.
68. Jakhmola, A.; Anton, N.; Vandamme, T. F., Inorganic Nanoparticles Based Contrast Agents for X-ray Computed Tomography. *Advanced healthcare materials* **2012,** *1* (4), 413-431.
69. Ashton, J. R.; West, J. L.; Badea, C. T., In vivo Small Animal Micro-CT Using Nanoparticle Contrast Agents. *Frontiers in pharmacology* **2015,** *6*, 256.
70. Liu, H.; Wang, H.; Guo, R.; Cao, X.; Zhao, J.; Luo, Y.; Shen, M.; Zhang, G.; Shi, X., Size-controlled Synthesis of Dendrimer-Stabilized Silver Nanoparticles for X-ray Computed Tomography Imaging Applications. *Polymer Chemistry* **2010,** *1* (10), 1677-1683.
71. Amendola, V.; Scaramuzza, S.; Litti, L.; Meneghetti, M.; Zuccolotto, G.; Rosato, A.; Nicolato, E.; Marzola, P.; Fracasso, G.; Anselmi, C., Magneto-Plasmonic Au-Fe Alloy Nanoparticles Designed for Multimodal SERS-MRI-CT Imaging. *Small* **2014,** *10* (12), 2476-2486.
72. Ton-That, C.; Foley, M.; Phillips, M. R., Luminescent Properties of ZnO Nanowires and as-Grown Ensembles. *Nanotechnology* **2008,** *19* (41), 415606.
73. Zhao, S.; Zhou, Y.; Zhao, K.; Liu, Z.; Han, P.; Wang, S.; Xiang, W.; Chen, Z.; Lü, H.; Cheng, B., Violet Luminescence Emitted from Ag-nanocluster Doped ZnO Thin Films Grown on Fused Quartz Substrates by Pulsed Laser Deposition. *Physica B: Condensed Matter* **2006,** *373* (1), 154-156.
74. Zeferino, R. S.; Flores, M. B.; Pal, U., Photoluminescence and Raman Scattering in Ag-doped ZnO Nanoparticles. *Journal of applied physics* **2011,** *109* (1), 014308.

75. Kachynski, A. V.; Kuzmin, A. N.; Nyk, M.; Roy, I.; Prasad, P. N., Zinc Oxide Nanocrystals for Nonresonant Nonlinear Optical Microscopy in Biology and Medicine. *The Journal of Physical Chemistry C* **2008,** *112* (29), 10721-10724.
76. Keevend, K.; Stiefel, M.; Neuer, A.; Neels, A.; Bertazzo, S.; Herrmann, I., Tb 3+-doped LaF 3 Nanocrystals for Correlative Cathodoluminescence Electron Microscopy Imaging with Nanometric Resolution in Focused Ion Beam-Sectioned Biological Samples. *Nanoscale* **2017,** *9* (13), 4383-4387.

TOC

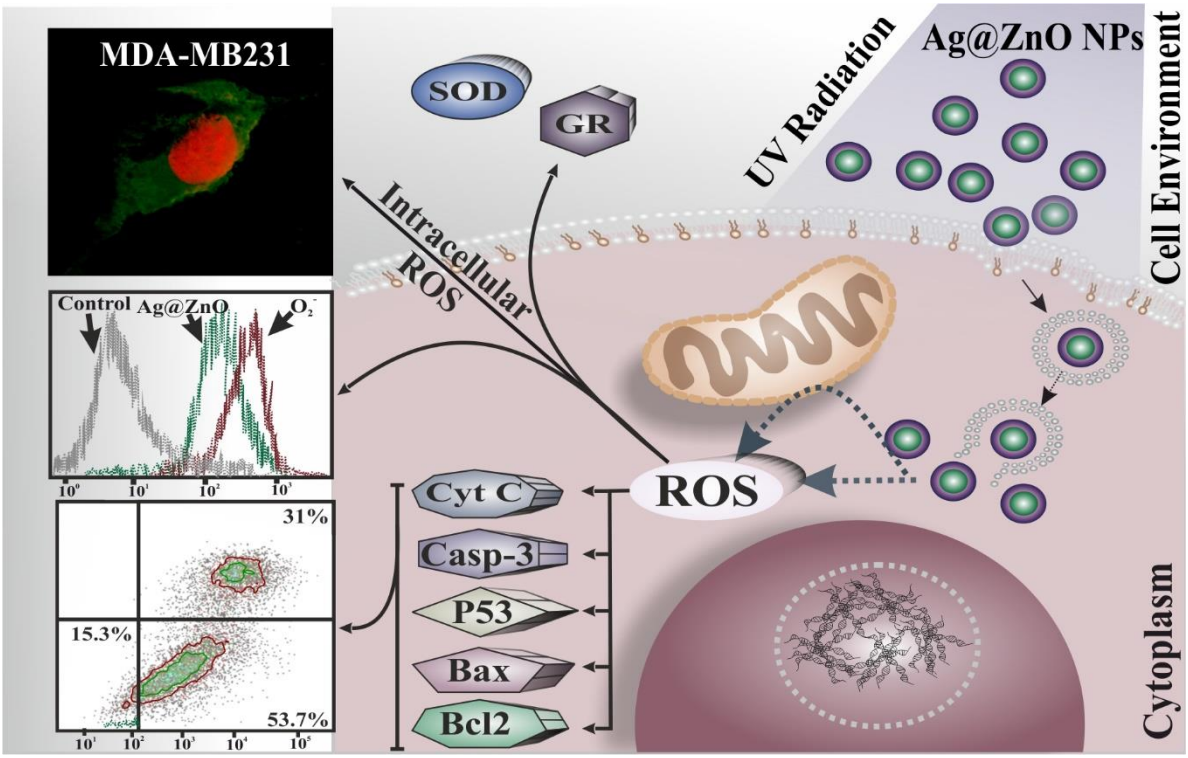
MDA-MB231
Control
Ag@ZnO
O_2^-
31%
15.3%
53.7%
SOD
GR
Intracellular ROS
UV Radiation
Ag@ZnO NPs
Cell Environment
ROS
Cyt C
Casp-3
P53
Bax
Bcl2
Cytoplasm